Supplementary information files for An investigation into the adsorption mechanism of n-butanol by ZIF-8: a combined experimental and ab initio molecular dynamics approach

Supporting Information

An investigation into the adsorption mechanism of n-butanol by ZIF-8: A combined experimental and *ab initio* molecular dynamics approach

Samuel P. Wallbridge[a], Stuart Archer[a], Mark. R. J. Elsegood[a], Jonathan L. Wagner[b], Jamieson K. Christie[c], Sandra E. Dann[a*]

[a]*Department of Chemistry, Loughborough University, Loughborough, U.K.*

[b]*Department of Chemical Engineering, Loughborough University, Loughborough, U.K.*

[c]*Department of Materials, Loughborough University, Loughborough, U.K.*

Email: S.E.Dann@lboro.ac.uk

Experimental

Materials

The reagents used in this study were 99 % 2-methylimidazole ($C_4H_6N_2$), 98+ % zinc acetate dihydrate ($Zn(OAc)_2.2H_2O$), 99.9 % methanol (CH_4O), 99+ % 1-pentanol ($C_5H_{12}O$) from Merck/Sigma Aldrich; 98 % zinc nitrate hexahydrate ($Zn(NO_3)_2).6H_2O$) and 99.9 % 1-butanol from Fischer Scientific; 99 % 1-hexanol ($C_6H_{14}O$), extra dry from Acros Organics; ethanol (C_2H_6O), 1-propanol (C_3H_8O), iso-butanol ($C_4H_{10}O$), tert-butanol ($C_4H_{10}O$). All chemicals were used as received without further purification.

Synthesis and Characterisation

ZIF-8 (MAF-4) (SOD-$Zn(Hmim)_2$, Hmim = 2-methylimidazole) was synthesised with different particle sizes by changing the synthesis conditions to preferentially enable fast or slow nucleation. Large particle ZIF-8 was synthesised by a solvothermal method adapted from Gao *et al.*[1] where 2-methylimidazole (0.3282 g, 4 mmol) and zinc acetate dihydrate (0.4380 g, 2 mmol) were separately dissolved in 11.3 g methanol. The two methanolic solutions were mixed and stirred for 15 minutes before being transferred to a PTFE-lined Parr Autoclave (125 ml), sealed and heated to 100 ^oC for 3 days. The vessel was allowed to cool to room temperature and the white solid collected by vacuum filtration, washed with methanol (3 x 50 ml) and dried in an oven at 80 ^oC for a further 3 days.

Small particles of ZIF-8 were synthesised by room temperature precipitation route. 2-methylimidazole (5.9112 g, 57 mmol) and zinc nitrate hexahydrate (5.3548 g, 18 mmol) were separately dissolved in 11.3 g methanol. The two methanolic solutions were mixed in a conical flask and stirred continuously for 1 h. The white solid was collected by centrifugation, washed 3 times with

methanol and dried in an oven at 80 °C for a further 3 days. Both samples were activated in a vacuum oven at 120 °C overnight, to remove residual solvent trapped inside the pores of the structure.

Powder X-ray diffraction data (PXRD) for spectra between 2θ 20-60 ° were collected on a Bruker D8 Discover in transmission geometry using monochromatic Co $K_{\alpha1}$ radiation (λ = 1.7890 $\dot{A}$). A step size of 0.015 ° was employed with a step time of 0.6 s. For low angle spectra, Powder X-ray diffraction data (PXRD) data were collected on a Bruker D8 Advance in reflectance geometry using monochromatic Cu $K_{\alpha1}$ radiation (λ = 1.5406 $\dot{A}$) and a quartz calibrated Lynxeye detector over a 2θ range of 5 – 35 ° with a step size of 0.015 °. A narrow primary focal slit of 0.2 mm was used to reduce the background caused by the Perspex sample holder and as a result a step time of 16 s was required for these measurements.

Combined thermogravimetric (TGA) and differential thermal analysis (DTA) data were collected on a TA Instruments SDT Q600 with two alumina crucibles (TA Instruments), one containing a reference and the other, the sample. A temperature range ramp method was applied, using an increasing temperature rate of 5 °C min^{-1}, over a range of 25 – 800 °C. A flow of air was regulated at 100 ml min^{-1} during analysis.

Surface area and pore volume data were determined using nitrogen adsorption/desorption isotherms obtained on a Micrometritics ASAP 2020. The samples were degassed under a nitrogen vacuum for 4 hours at 150°C prior to analysis. The weight of the sample after degassing was used in all further calculations. BET surface areas were calculated over a partial pressure range of 0.005-0.0005 (p/p^o). The total pore volume was measured with a single point on the adsorption isotherm at p/p^0 = 0.994 cm^3 g^{-1}.

Attenuated total reflectance infrared (ATR-IR) were collected using a Shimadzu IT Affinity-1 fitted with an ATR stage. The spectra were recorded between 400 - 4000cm^{-1} with a resolution of 4 cm^{-1} for 64 scans, both background and sample spectra.

Raman (R) data were collected between 100 - 4000 cm^{-1} using a Horiba Jobin Yvon HR LabRAM system in the backscatter configuration with a laser line at 633 nm originating from an argon ion laser. The laser was focused onto the sample to a spot size of around 1 µm at 100 % power during analysis, as no sample decomposition was observed under these conditions.

Scanning Electron Microscopy (SEM) was carried out at the Loughborough Materials Characterisation Centre (LMCC) on a Jeol JSM 7100F Field Emission SEM instrument with a lower electron detector, producing secondary electron imaging. Samples were dispersed on a carbon sample

holder and coated with Au/Pd for 90 s to prevent charging of the sample. An accelerating voltage of either 2 or 5 kV was applied to the electron beam, and a working distance of 10.0 mm was utilised. Micrographs were collected up to a maximum magnification of 40,000.

Adsorption experiments

The liquid-phase adsorption isotherms of the two ZIF-8 sample towards 1-butanol have been studied across the concentration range 0.05 - 5 wt % by adding 0.2 g ZIF-8 to a small vial with 5 ml aqueous alcohol solution and agitating at 300 rpm on Fine PCR FMS3 multishaker for 24 h. The sample was collected by centrifugation, liquid fraction decanted and filtered through a 0.45 or 0.22 μm syringe filter, depending on the particle size.

For experiments carried out with ZIF-8 synthesised solvothermally, analysis was carried out using a Hitachi Chromaster HPLC fitted with an Agilent MetaCarb 67H Organic Acids Column (H^+ form) at 55 °C and a mobile phase flow rate of 0.8 ml min^{-1}. A Ce Instruments Ltd Refractive Index (RI) detector was used to determine the concentration of butanol present in the liquid samples. For experiments carried out with ZIF-8 synthesised by room temperature precipitation, analysis was carried out using a Nexis GC-2030 Gas Chromatograph with a Shimadzu Dielectric-Barrier Discharge Ionisation Detector (BID). The column used was an Agilent DB-WAX column with a carrier gas of He flowing at a rate of 50 ml min^{-1}. Samples were diluted 10-fold in pure methanol before injection onto the column. The column was heated using a temperature programme of 35 °C for 4 mins, followed by a ramp at 10 °C min^{-1} to 95 °C.

The equilibrium adsorption capacity, Qe, of ZIF-8 after 24 h is defined as grams of adsorbate per gram of adsorbent, calculated using equation 1:

$$Q_e = \frac{(C_o - C_e)V}{M} \quad (1)$$

Where C_o is the starting concentration of solution (g L^{-1}); C_e is the equilibrium concentration of solution (g L^{-1}); V is the volume of solution (L); M is the mass of adsorbent (g).[1]

The Langmuir model is then fitted to adsorption data to determine the maximum saturation capacity for n-butanol, as summarised in equation 2 below where:

$$Q = \frac{Q_{max} k C_e}{1 + k C_e}$$

(2)

Q_{max} is the saturation adsorption capacity (g g^{-1}), k is the Langmuir coefficient (L g^{-1}) and C_e is the equilibrium concentration of the solution (g g^{-1}).[2]

The linear derivation of the Langmuir model is as follows in equation 3:

$$\frac{C_e}{Q_e} = \frac{1}{k Q_{max}} + \frac{C_e}{Q_{max}}$$

(3)

Diffuse reflectance infrared Fourier transform spectroscopy (DRIFTS)

DRIFTS experiments were carried out at the UK Catalysis Hub laboratories, Harwell, using an Agilent Technologies Cary 600 Series FTIR Spectrometer with MTC detector coupled to a Hiden Analytical QGA Mass Spectrometer. Spectra were recorded using Agilent Resolutions Pro software. Pre-adsorbed ZIF-8 was prepared by soaking ca. 50 mg of as prepared ZIF-8 in 1 ml of pure n-butanol for 1 h on a watch glass; excess liquid was then allowed to dry from the surface. Approximately 20 mg of the pre-adsorbed sample was placed into the Harrick reaction chamber and flushed with N_2 for 10 minutes before heating from 30 to 300 °C at a ramp rate of 5 °C min^{-1}. Spectra were recorded *in situ* every 10 °C in order to monitor the desorption of n-butanol.

Density Functional Theory

Molecular simulations have been used to determine the optimised structure of ZIF-8 and subsequently study the adsorption characteristics of n-butanol within the framework. Calculations performed in this work are based on a first-principles Density Functional Theory (DFT) approach employing the QUICKSTEP module of the CP2K program.[3] The module uses the Gaussian Plane Wave (GPW) method for treatment of electrostatic interactions. The code uses Gaussian type basis sets and employs Goedecker-Teker-Hutter (GTH) pseudopotentials for the core electrons. For each atom, the TZVP-MOLOPT-GTH basis set is used, except for Zn which uses the DZVP-MOLOPT-SR-GTH basis set. A planewave cut-off value of 450 Ry was applied to all static and molecular dynamics calculations. Calculations were performed using the Generalised Gradient Approach (GGA) in the form of the Perdew-Burke-Ernzerhof (PBE) exchange-correlation functional.[4] To minimise the total ground-state energy the orbital transformation method was used (OT) with direct inverse in the iterative subspace

(DIIS) minimiser. The self-consistency loop was considered converged when the energy change was less than 1 x 10^{-10} Hartree for the initial geometry optimisation of the structure; this was relaxed to 1 x 10^{-7} Hartree for dynamic calculations and cell optimisations. As DFT does not account for the dispersion (van der Waals') interactions, dispersion corrections were included in the form of Grimme's DFT-D2.[5]

All calculations were performed using the full ZIF-8 cubic unit cell; starting coordinates were acquired from crystallographic data reported by Wu et. al (CDCC OFERUN) which consists of 12 zinc, 96 carbon, 120 deuterium (substituted for hydrogen atoms with the same atomic coordinates) and 48 nitrogen atoms.[6] Periodic boundary conditions were applied in xyz directions with unit cell parameters a = 16.9901 $\dot{A}$ and α = 90 °. The energy of the system (in the absence of adsorbed molecules) was initially minimised by geometry optimisation at constant temperature and pressure, where atomic coordinates only were relaxed. The conjugate gradient (CG) optimisation method has been used for all optimisation calculations. The convergence for geometry and forces were set as 0.0003 Bohr and 0.000045 Hartree/Bohr, respectively. The optimised ZIF-8 coordinates were used in all following molecular dynamics simulations.

Ab initio molecular dynamics simulations were caried out to investigate the behaviour of n-butanol inside the ZIF-8 cages. Two simulations were carried out in which 6 and 7 butanol molecules were placed inside the pore; the systems were first equilibrated at 500 K for 10 ps to randomise the butanol positions. The production run was then carried out for a further 15 ps at 300 K to allow the butanol to adopt its global minimum position within the cage. The simulations were caried out with a time step of 0.5 fs using the Nose-Hoover chain ensemble with NVT thermostat.

Following the 15 ps production run, a cell optimisation was performed on the structure with adsorbed species, where both atomic coordinate and cell dimensions were allowed to relax; the symmetry was fixed as cubic. During cell optimisation calculations, the convergence criteria for geometry and forces were increased to 0.003 Bohr and 0.0045 Hartree/Bohr, respectively, with a pressure tolerance of 130 bar. Identical cell optimisation calculations were carried out on the ZIF-8 framework in the absence of adsorbed species, and for the final butanol coordinates without the presence of the framework (simulation box size 40 x 40 x 40 $\dot{A}$). The adsorption energy per butanol molecule could then be calculated from the below equation:

$$E_{ads} = \frac{(E_{ZIF+nBuOH} - E_{ZIF} - nE_{BuOH})}{n}$$

where $E_{ZIF+nBuOH}$ is the energy of ZIF-8 with n-butanol adsorbed inside the cage, E_{ZIF} is the energy of ZIF-8 without the presence of butanol and nE_{BuOH} is the energy of n-butanol without the presence of the ZIF-8 cage.[7]

Charge density analysis was carried out by computing the binding induced density difference utilising the CP2K tool "cubecruncher" to manipulate cube files.

$$\rho_{induced} = \rho_{ZIF+BuOH} - \rho_{BuOH} - \rho_{ZIF}$$

Solid State NMR Measurements

Solid state NMR measurements were recorded on a JEOL ECZ-500 500 MHz NMR spectrometer equipped with a broadband 3.2 mm MAS solid state probe. Samples were packed into a 3.2 mm zirconia rotor with spacer, Vespel end caps, and spun at 15 KHz. The 90 degree pulse widths were measured for ^{1}H (3.2 µs) and ^{13}C (3.1 µs), and these values used for direct polarization (MAS) and cross polarisation (CP-MAS) experiments. T1ρ was measured for ^{1}H and ^{13}C nuclei using a standard saturation recovery experiment prior to MAS/CP-MAS data collection.

1H MAS experiments were obtained using 8 scans, 1024 data points giving an 8.2 ms acquisition time, a recycle delay of 2 s, and an x-offset of 0 ppm with a sweep of 200 ppm.

13C CP-MAS experiments were obtained with a cross polarisation mixing time of 1.2 ms with ramped gradient, 256 scans, 2048 data points giving an acquisition time of 32 ms, a recycle delay of 10 s, and an x-offset of 100 ppm with a sweep of 300 ppm. Decoupling was carried during acquisition using TPPM noise at 15.2 dB.

2D 13C-1H HETCOR experiments on ZIF-8 with adsorbed n-butanol were obtained from direct observation of 13C with 1H in the indirect dimension. Compared to previous related work by Du *et. al* it was found that a longer mixing time of 19.6 ms was required to observe correlations from the n-butanol with the ZIF framework.[8] A total of 16384 scans were collected, comprising of 64 scans, 4096 data points, x-offset of 100 ppm with a 200 ppm sweep in the direct axis; and 256 indirect axis data points with an offset of 0 ppm with a 20 ppm sweep. Decoupling was carried during acquisition using TPPM noise at 15.2 dB.

13C T_1r values were measured using a saturation recovery experiment at 15 kHz MAS, with 0.1 s saturation interval, 16384 data points and 64 scans per interval, 1 second intervals between 1-40 seconds, relaxation delay of 10 s. Collected data was fitted using Delta 5.3.1 software and a weighted linear saturation recovery function.

Extended data

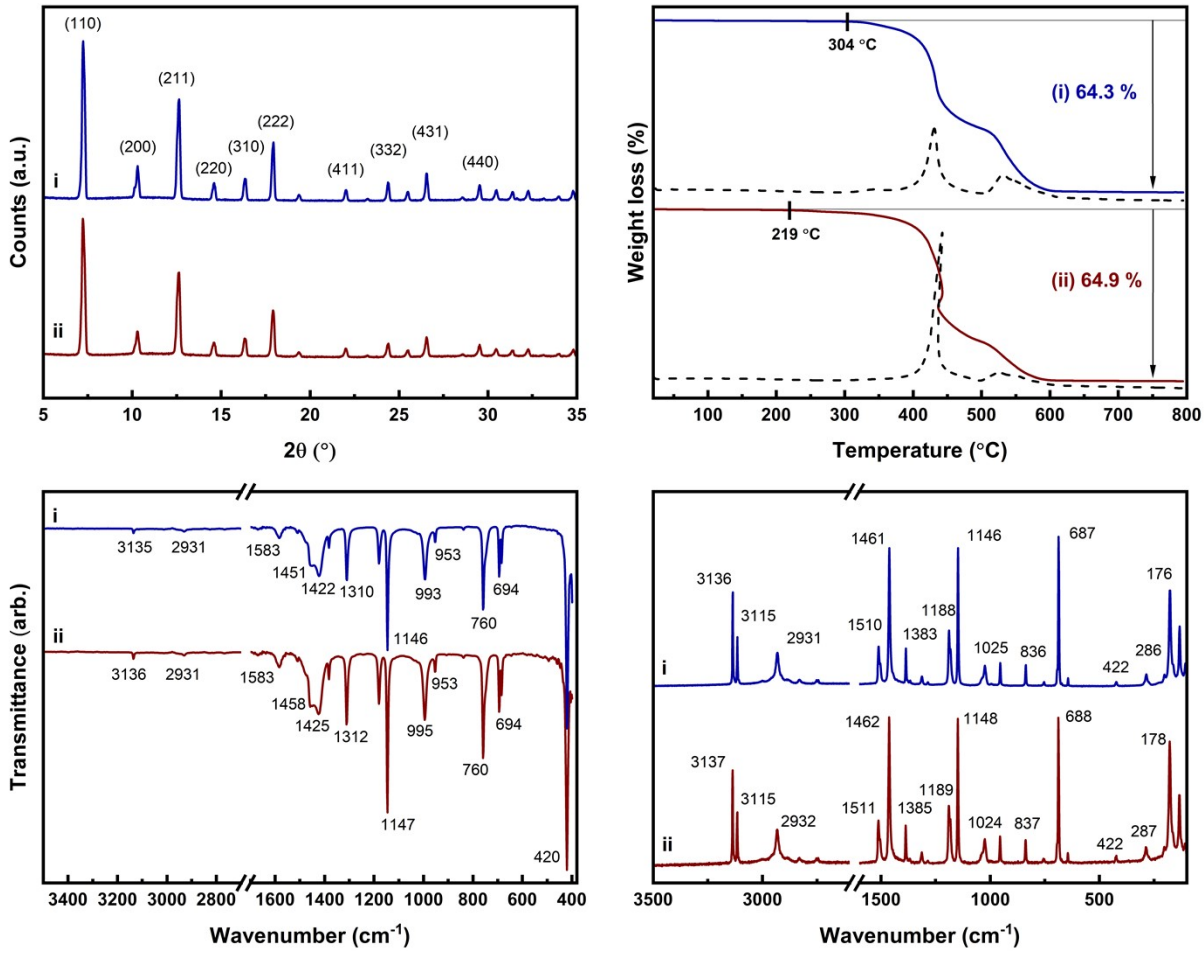

Figure S1. Data collected of ZIF-8 synthesised by (i) solvothermal (shown in blue) and by (ii) room temperature precipitation (shown in red) methods. **(a)** powder X-ray diffraction patterns collected with Cu $K_{\alpha 1}$ radiation (λ = 1.5406 $\AA$), **(b)** thermogravimetric analysis (TGA) mass loss data with decomposition to ZnO and differential thermal analysis (DTA) data shown as dashed lines, **(c)** ATR-infrared absorption and **(d)** Raman spectra.

Powder X-ray diffraction data shown in **Fig. S1(a)** for ZIF-8 synthesised by solvothermal and room temperature precipitation methods shows that both samples are pure phase, crystalline ZIF-8 materials. Reflections are indexed according to data collected by Wu *et. al.* (CCDC 652302) and there is good agreement between both patterns.[6]

Thermogravimetric analysis (TGA) carried out in air **(Fig. S1(b))** shows that both ZIF-8 samples exhibit similar decomposition profiles, with no weight loss observed below 200 °C, demonstrating that the pores are free from the presence of any solvent, removed during the activation step. The plots

show that ZIF-8 synthesised by the room temperature precipitation method has a lower decomposition onset temperature of 219 °C compared to the solvothermal sample (304 °C). Both samples undergo a two-step decomposition; differential thermal analysis (DTA) data shows a large exothermic transformation at 431 and 443 °C for solvothermal and RT samples, respectively, followed by a second broader and less exothermic transformation at 526 °C for both samples. The samples have fully decomposed to pure ZnO by 600 °C, as confirmed by powder X-ray diffraction **(Fig. S2)**. The total observed weight losses are 64.3 (± 0.9) and 64.9 (± 0.5) for solvothermal and RT methods, respectively. The slightly higher observed mass loss for the room temperature sample might be explained by small amounts of 2-methylimidazole starting material remaining in the sample, reflecting the lower onset decomposition temperature for this sample.

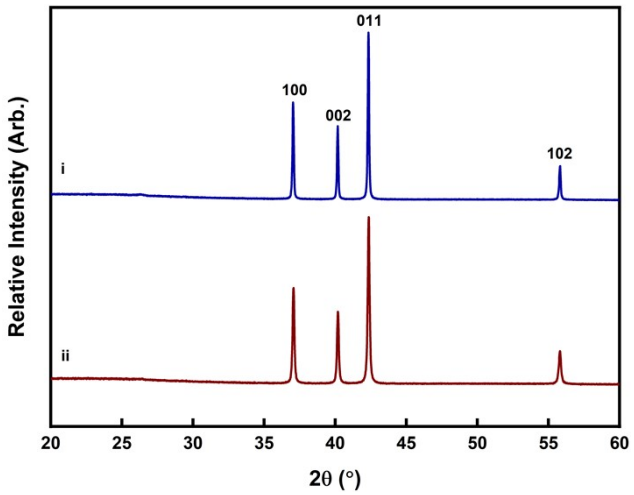

Figure S2. Powder X-ray diffraction patterns collected with Co $K_{\alpha 1}$ radiation (λ = 1.7889 Å) of the zinc oxide products obtained after thermogravimetric analysis of the ZIF-8 synthesised (i) solvothermally and (ii) by room temperature precipitation method. The hkl assignments are given for the reflections of zinc(II) oxide (ICSD 26170).[9]

Elemental analysis data provided in **Table S1** show that the compositions of ZIF-8 synthesised by both methods are very similar; with the sample synthesised at room temperature exhibiting only very slightly higher carbon, hydrogen and nitrogen contents. In both cases, the nitrogen content is lower than the theoretical value for ZIF-8 and slightly outside of the accepted error for this technique of ±0.4 %.[10]

Table 1. Thermogravimetric Analysis (TGA) and elemental analysis (CHN) data for ZIF-8 synthesised by solvothermal and room temperature precipitation routes. Theoretical values are based on the ZIF-8 formula $C_8H_{10}N_4Zn$. TGA data were collected in triplicate, whilst elemental analyses were collected in duplicate.

	Thermogravimetric Analysis (TGA)				Elemental Analysis					
	End Phase	Mass Loss (%)		ESD	%C		%N		%H	
		Exp.	Theo.		Exp.	Theo.	Exp.	Theo.	Exp.	Theo.
Solvothermal	ZnO	64.3	64.2	0.9	41.9	42.2	24.0	24.6	4.0	4.4

RT		64.9		0.5	42.0		24.1		4.2	

Spectroscopic techniques (IR/Raman) included in **Fig. S1(c)** and **Fig. S1(d)** show characteristic bands of ZIF-8 for both samples with assignments made based on literature data; the spectra are almost identical for both samples.[11,12] The aromatic ν_{sym} C-H is present at ca. 3135 cm^{-1} for both IR/R spectra, with an additional sharp band present at ca. 3115 cm^{-1} in the Raman spectra. The ν_{asym} C-H of the methyl group is again present for both IR and R at ca. 2931 cm^{-1}. The broad band at 1583 cm^{-1} in both IR spectra is assigned to ν C-C and is Raman inactive. The Raman spectra have a relatively weak band at 1510 cm^{-1} that is also assigned to C-C stretching and is only weak in the IR spectra. The δ_{asym} (CH_3) band is present in both spectra at approx. 1460 cm^{-1}; δ (C-H) aromatic in-plane bend at ca. 1422 cm^{-1} in the IR only; δ_{sym} (CH_3) at ca. 1380 cm^{-1} in both and a further δ (C-H) aromatic in-plane bend at ca. 1285 cm^{-1} in the R only. δ (C-H) out-of-plane bands are present at ca. 1024, 955 and 690 cm^{-1} in both spectra. The Zn-N ring stretch is found at ca. 420 cm^{-1} in both IR and R, however is very weak in the Raman.

N_2 adsorption/desorption analysis **(Fig. S3)** shows that both L- and S-ZIF-8 display type II isotherms with a sharp uptake of N_2 in the microporous region. S-ZIF-8 exhibits a larger uptake of N_2 than L-ZIF-8 which is reflected in a slightly larger estimated surface area of 1433 $m^2\ g^{-1}$ compared to 1373 $m^2\ g^{-1}$ for S-ZIF-8 and L-ZIF-8, respectively. This increase in surface area for S-ZIF-8 is explained by the larger contribution of external surface area compared to internal crystal volume with the decrease in crystal size. The total pore volume calculated for L-ZIF-8 is 0.66 $cm^3\ g^{-1}$ compared to 0.71 $cm^3\ g^{-1}$; the observed increase total pore volume is a result of a small contribution from interparticle meso- and macro- porosity **(Fig S3(b))** present in the sample with small, uniform crystals.

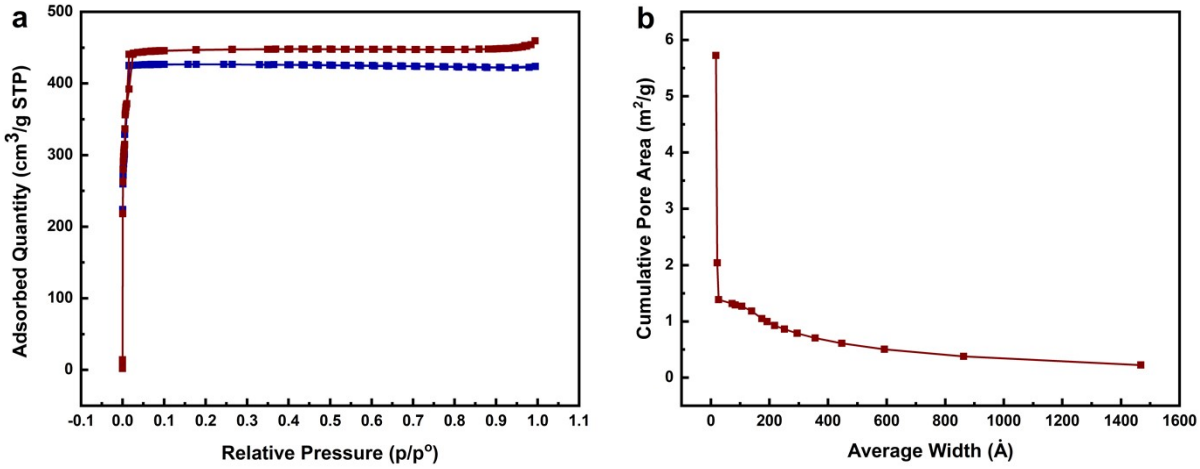

Figure S3. (a) N_2 adsorption/desorption isotherms of L-ZIF-8 (blue) and S-ZIF-8 (red) displaying type II isotherms characteristic of a microporous material. **(b)** Barrett-Joyner-Halenda (BJH) pore size distribution collected from N_2 adsorption data of S-ZIF-8.

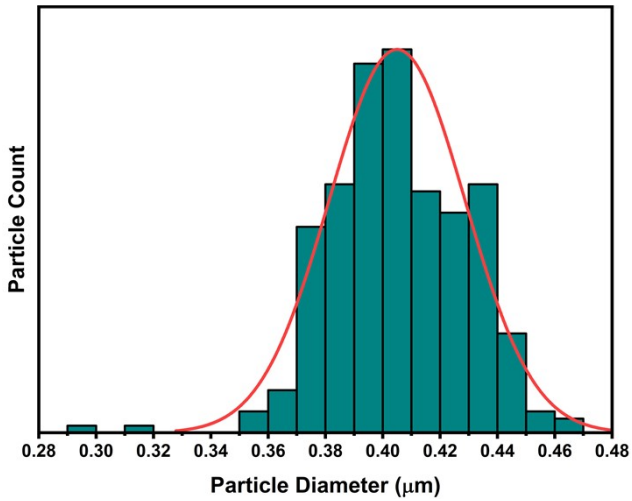

Figure S4. Particle size distribution of ZIF-8 synthesised by room temperature chemical precipitation method (S-ZIF-8) determined by measuring the diameter of 300 particles using the SEM micrograph shown in Fig. 2(a) and utilising the software package ImageJ.

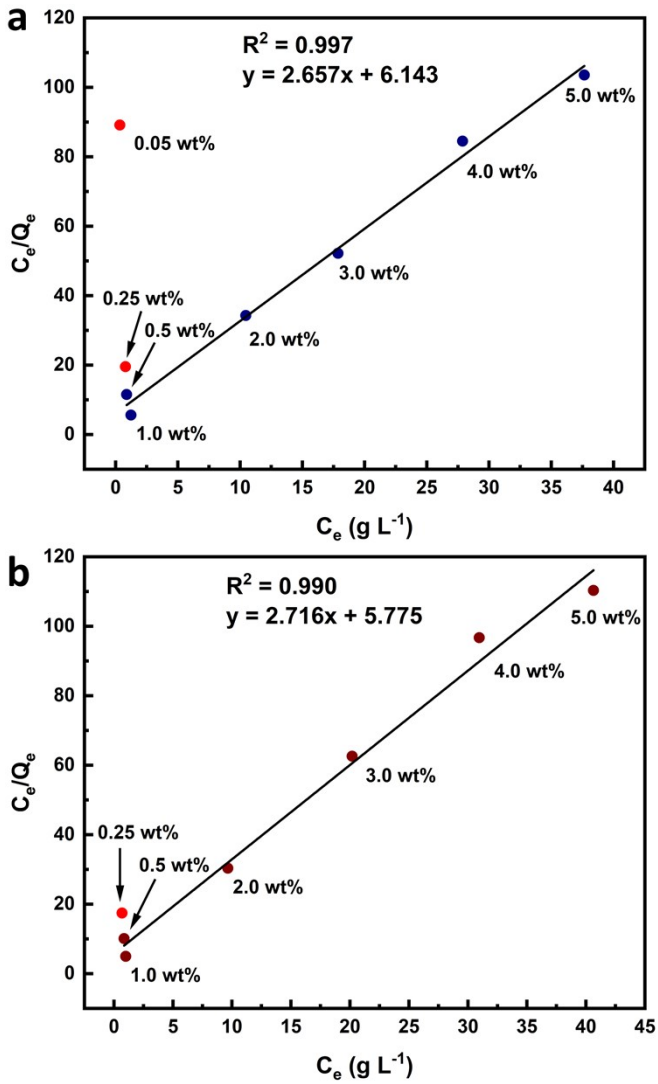

Figure S5. Linear derivation of the Langmuir model for liquid-phase n-butanol adsorption isotherm data for **(a)** L-ZIF-8 and **(b)** S-ZIF-8. The gradient is equal to $1/Q_{max}$, whilst the y-axis intercept is equal to $1/Q_{max}k$. Data points shown in red are excluded as they do not fit the Langmuir model.

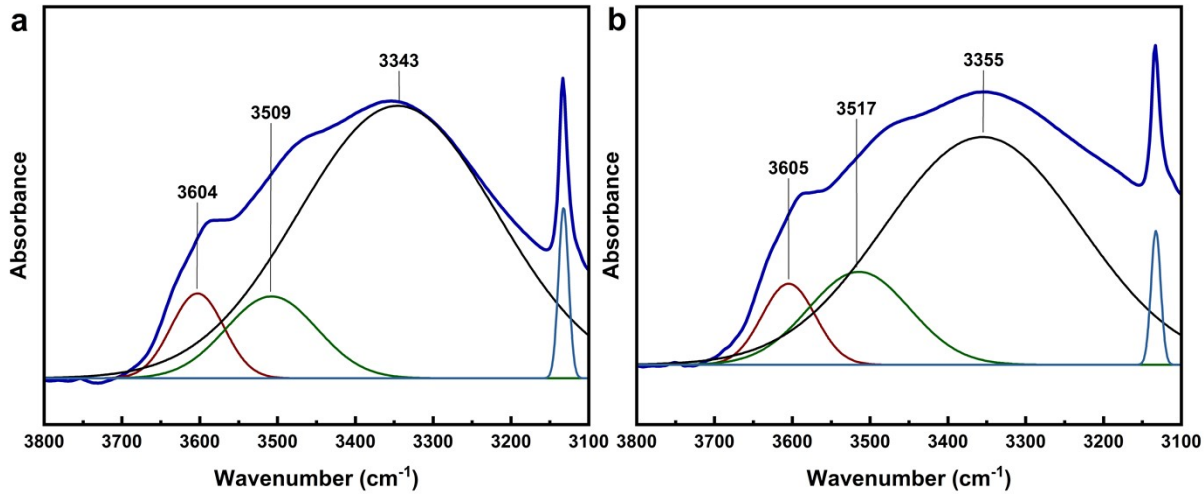

Figure S6. Gaussian deconvolution of bands in the O-H stretching region of DRIFTS spectra collected for **(a)** L-ZIF-8 and **(b)** S-ZIF-8 with pre-adsorbed n-butanol species at 30 °C.

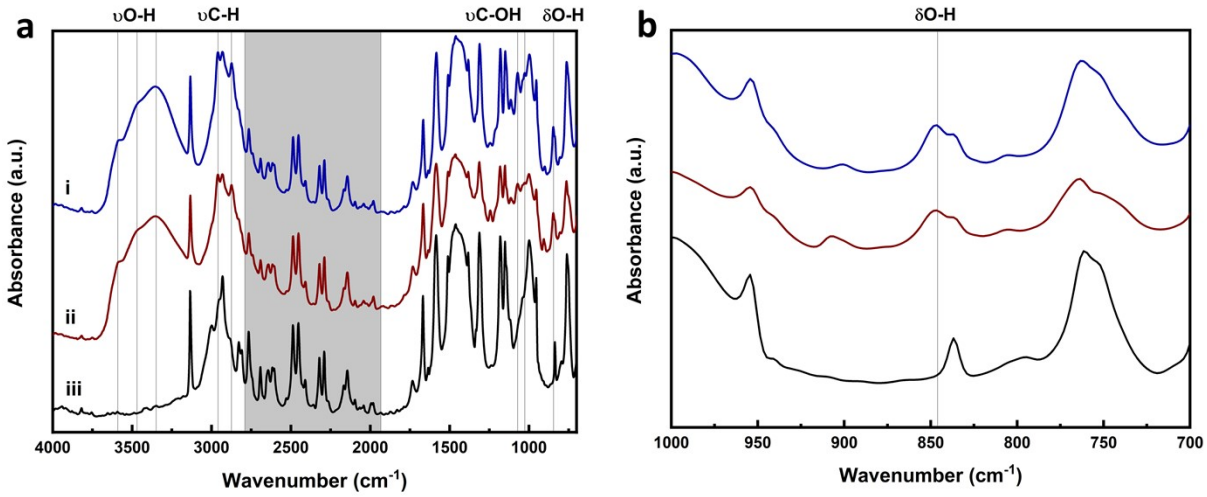

Figure S7. DRIFTS spectra collected at 30 °C of ZIF-8 samples (i) L-ZIF-8 with pre-adsorbed n-butanol, (ii) S-ZIF-8 with pre-adsorbed n-butanol and (iii) blank L-ZIF-8 sample for reference. **(a)** Full spectra, where solid vertical lines denote vibrational modes of adsorbed n-butanol species. The shaded region contains spectral artefacts that are assumed to be a result of Fresnel reflectance, where the beam of light interacts with the surface only. This phenomenon can be lessened by improved sample preparation (packing, sample dilution), but are also a result of the inherent refractive index and absorption coefficients of the sample.[13,14] **(b)** Spectra for samples (i), (ii) and (iii) with the region from 1000 – 700 cm^{-1} enlarged in order to highlight the additional $\delta O-H$ band present in both sample with adsorbed n-butanol.

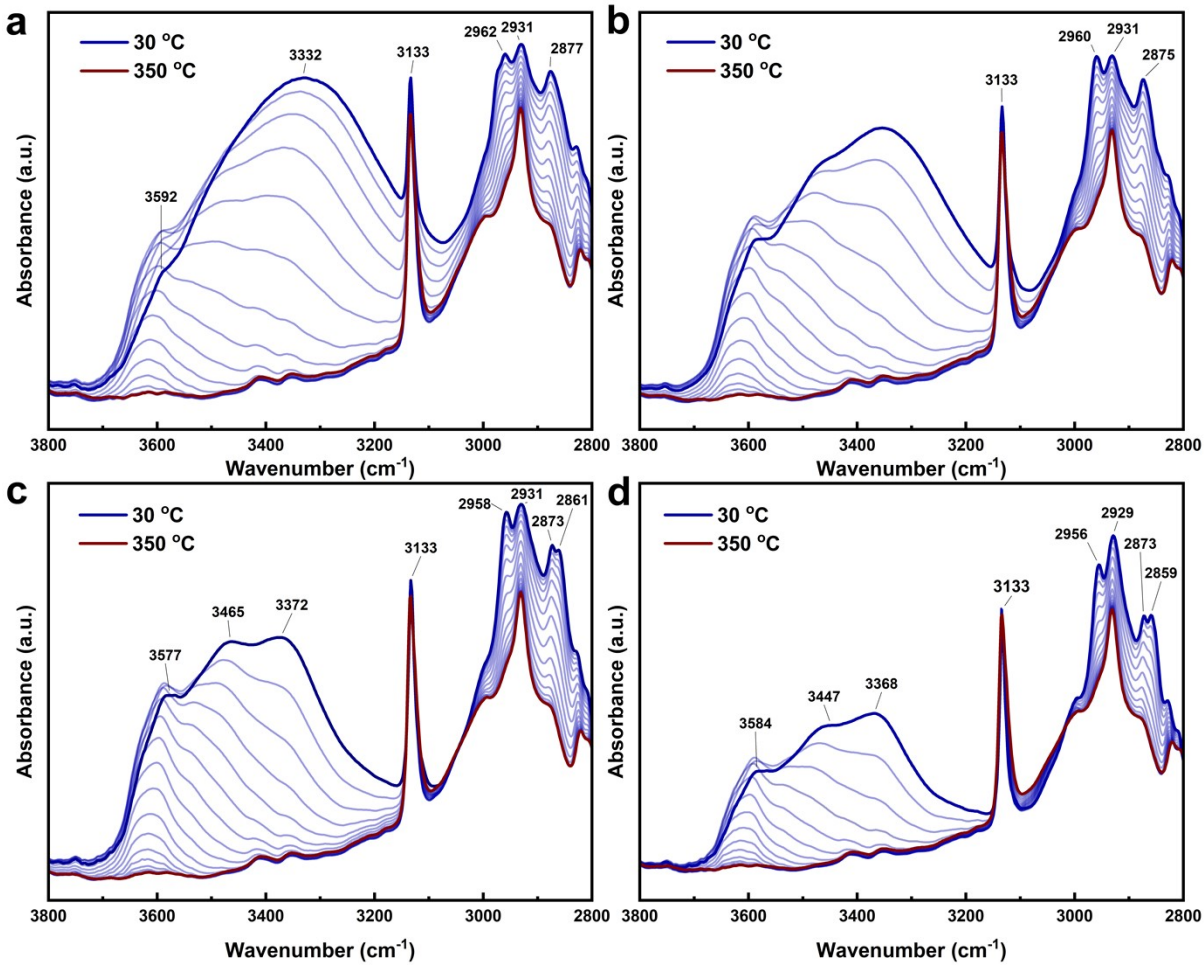

Figure S8. Diffuse reflectance infrared Fourier transform spectroscopy (DRIFTS) spectra collected during *in situ* desorption experiments carried out under a N_2 atmosphere for L-ZIF-8 with pre-adsorbed **(a)** 1-propanol, **(b)** 1-butanol, **(c)** 1-propanol, and **(d)** 1-hexanol. A constant temperature ramp of 5 ^{o}C min^{-1} was applied to the sample cell and spectra recorded every 10 °C up to 350 °C, showing the loss of alcohol bands as desorption occurs.

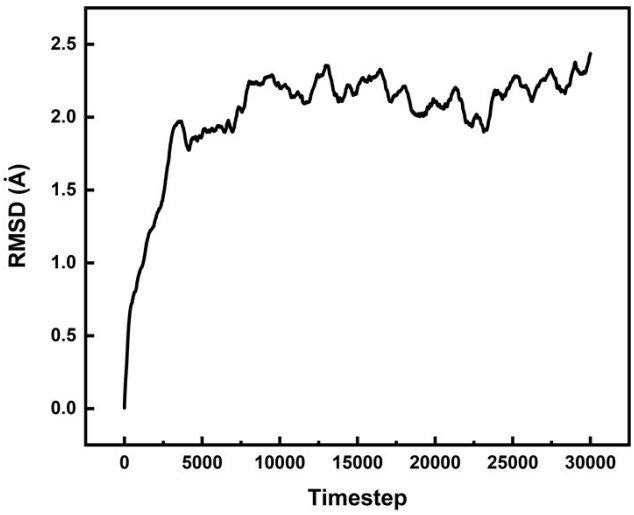

Figure S9. Root-mean-square deviation (RMSD) of the n-butanol coordinates from their starting positions, during *ab initio* molecular dynamics simulation of 7 butanol molecules adsorbed in the ZIF-8 cages at 300 K, over the course of 30,000 simulation timesteps. The plots shows that there is little movement of the butanol molecules in the final 10,000 steps. N.B Each timestep is equal to 0.5 ps.

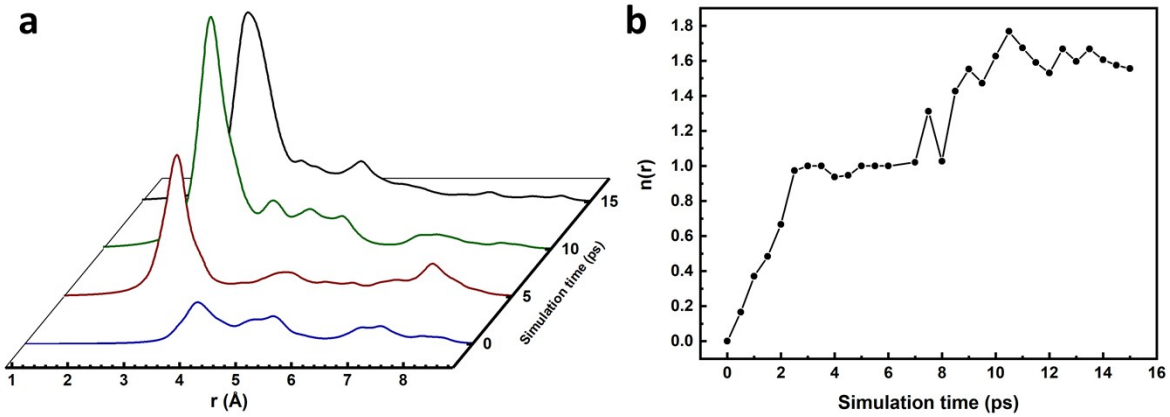

Figure S10. Analysis of hydrogen bonding over the course of the *ab initio* molecular dynamics simulation of 6 butanol molecules inside the ZIF-8 cages. **(a)** Shows how the radial distribution function (RDF), g(r), for the intermolecular O-O distance varies between 0 to 9 $\dot{A}$ averaged over 1 ps of time starting at 0, 5, 10 and 15 ps into the simulation, and shown in blue, red, green and black, respectively. **(b)** Average coordination number, n(r), of each oxygen atom to neighbouring oxygen atoms at a distance below 3.31 $\dot{A}$.

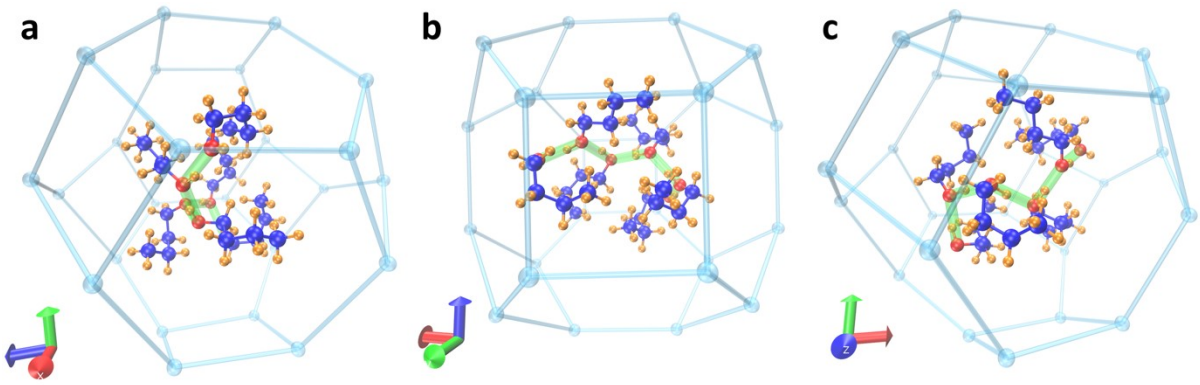

Figure S11. Arrangement of six butanol molecules inside the ZIF-8 framework after production run at 300 K for 15 ps of molecular dynamics simulation viewed along the **(a)** x-axis, **(b)** y-axis and **(c)** z-axis. The ZIF-8 β-cage is represented by just the zinc framework atoms in light blue with organic imidazole linkers excluded for clarity. Carbon atoms of butanol molecules are shown in deep blue, hydrogen atoms in orange and oxygen atoms in red. Hydrogen bonding between butanol molecules is shown by highlighting O-O distances less than or equal to 3.31 $\dot{A}$ in green.

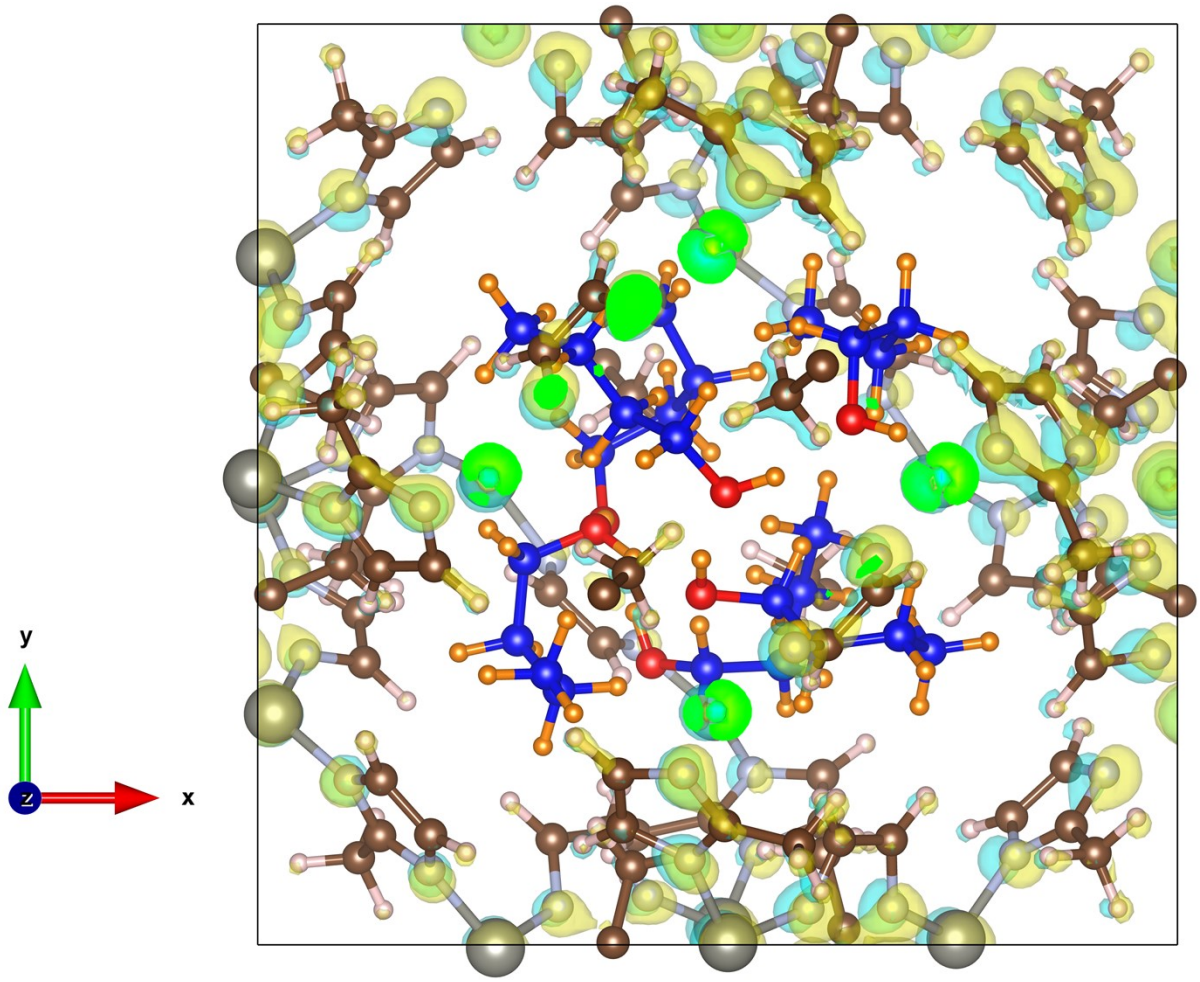

Figure S12. Charge density plot of the optimised coordinates after 15 ps molecular dynamics simulation at 300 K with six butanol molecules inside the ZIF-8 framework. Areas of charge accumulation are shown in yellow, and areas of charge depletion are shown in blue, with an iso surface value of 0.035 e/$\dot{A}^3$. The only areas of charge accumulation or depletion are on the ZIF-8 framework and there is no evidence of charge transfer between the butanol molecules and the cage. Butanol atoms: carbon in blue, hydrogen in orange and oxygen in red. Framework atoms: carbon in brown, nitrogen in light blue and zinc in grey

References

1 C. Gao, Q. Shi and J. Dong, *CrystEngComm*, 2016, **18**, 3842–3849.

2 T. D. Kühne, M. Iannuzzi, M. Del Ben, V. V. Rybkin, P. Seewald, F. Stein, T. Laino, R. Z. Khaliullin, O. Schütt, F. Schiffmann, D. Golze, J. Wilhelm, S. Chulkov, M. H. Bani-Hashemian, V. Weber, U. Borštnik, M. Taillefumier, A. S. Jakobovits, A. Lazzaro, H. Pabst, T. Müller, R. Schade, M. Guidon, S. Andermatt, N. Holmberg, G. K. Schenter, A. Hehn, A. Bussy, F. Belleflamme, G. Tabacchi, A. Glöß, M. Lass, I. Bethune, C. J. Mundy, C. Plessl, M. Watkins, J. VandeVondele, M. Krack and J. Hutter, *Journal of Chemical Physics*, 2020, **152.**

3 J. P. Perdew, K. Burke and M. Ernzerhof, *Phys Rev Lett*, 1996, **77**, 3865–3868.

4 S. Grimme, *Journal of Chemical Physics*, 2006, **124.**

5 H. Wu, W. Zhou and T. Yildirim, *J Am Chem Soc*, 2007, **129**, 5314–5315.

6 H. P. Paudel, W. Shi, D. Hopkinson, J. A. Steckel and Y. Duan, *React Chem Eng*, 2021, **6**, 990–1001.

7 Y. Du, K. Mao, B. Wooler, A. K. Sharma, D. Colmyer, M. Nines and S. C. Weston, *Journal of Physical Chemistry C*, 2017, **121**, 28090–28095.

8 S. C. Abrahams and J. L. Bernstein, *Acta Crystallogr B*, 1969, **25**, 1233–1236.

9 R. E. H. Kuveke, L. Barwise, Y. Van Ingen, K. Vashisth, N. Roberts, S. S. Chitnis, J. L. Dutton, C. D. Martin and R. L. Melen, *ACS Cent Sci*, 2022, **8**, 855–863.

10 D. A. Carter and J. E. Pemberton, *Journal of Raman Spectroscopy*, 1997, **28**, 939–946.

11 N. P. G. Roeges, *A Guide to the Complete Interpretation of Infrared Spectra of Organic Structures*, John Wiley & Sons Ltd., Chichester, 1994.

12 J. P. Blitz, in *Modern techniques in applied molecular spectroscopy*, Wiley, 1998, pp. 185–219.

13 T. Armaroli, T. Bécue and S. Gautier, *Oil & Gas Science and Technology-Rev. IFP*, 2004, **59**, 215–237.